Absolute cross sections for excitation of the $2s\,^2S \rightarrow 2p\,^2P$ transition in B^{2+} and for electron-impact single ionization of B^{2+}

O. Woitke, N. Djurić, and G. H. Dunn
JILA, University of Colorado and National Institute of Standards and Technology, Boulder, Colorado 80309-0440

M. E. Bannister
Physics Division, Oak Ridge National Laboratory, Oak Ridge, Tennessee 37831-6372

A. C. H. Smith
Department of Physics and Astronomy, University College London, London WC1E 6BT, United Kingdom

B. Wallbank
Department of Physics, St. Francis Xavier University, Antigonish, Nova Scotia, Canada B2G 2W5

N. R. Badnell
Department of Physics and Applied Physics, University of Strathclyde, Glasgow G4 0NG, United Kingdom

M. S. Pindzola
Department of Physics, Auburn University, Auburn, Alabama 36849
(Received 30 June 1998)

Absolute cross sections for electron-impact excitation of the $2s\,^2S \rightarrow 2p\,^2P$ transition of B^{2+} measured between 5.4 and 7.0 eV are presented. The results are in good agreement with the *R*-matrix-with-pseudostates (RMPS) calculation of Marchalant *et al.* [J. Phys. B **30**, L435 (1997)]. Also presented are cross sections for electron-impact single ionization of B^{2+}, including measurements between 25 and 200 eV and calculations using the RMPS and time-dependent close-coupling methods. The measured ionization cross sections are about 14% higher near the peak than previous measurements by Crandall *et al.* [Phys. Rev. A **34**, 1757 (1986)], but agree well with experimental data of Hofmann *et al.* [Z. Phys. D **16**, 113 (1990)] and with the present and other theoretical predictions. [S1050-2947(98)01212-8]

PACS number(s): 34.80.Kw

I. INTRODUCTION

Experimental cross sections for electron-impact excitation and ionization of ions are of importance in fields concerned with the modeling of high-temperature plasmas, such as fusion and astrophysics, where the large amount of data needed is mostly supplied by theoretical methods. The experimental cross sections serve as benchmarks for these predictions and can be used to set up scaling rules for isoelectronic sequences. The lithium isoelectronic sequence has been the focus of a number of measurements, (see, e.g. [1–6]) and is of particular interest because transitions in Li-like ions are commonly used in plasma diagnostics.

In this paper measurements of cross sections for the electron-impact excitation of the $2s\,^2S \rightarrow 2p\,^2P$ transition in B^{2+} are presented and compared with an *R*-matrix-with-pseudostates (RMPS) calculation by Marchalant *et al.* [7]. Also presented are experimental data and calculations for the electron-impact single ionization of B^{2+} with comparisons to previous experimental results of Crandall *et al.* [3] and Hofmann *et al.* [4]. The present ionization results are also compared to other calculations [7,8].

II. EXPERIMENT

A. Excitation

The absolute electron-impact excitation cross sections for the dipole-allowed transition $2s \rightarrow 2p$ in $^{11}B^{2+}$ were measured at the Oak Ridge National Laboratory (ORNL) using the JILA/ORNL merged electron-ion beams energy loss technique. Full details of the method are given elsewhere [5,9] and only a brief description is included here. A schematic of the experimental setup is shown in Fig. 1. In the crossed **E** and **B** fields of a trochoidal analyzer (''merger''), an electron beam performs two gyrations resulting in a displacement perpendicular to its original direction, while preserving its direction and velocity. Upon leaving the merger, the electron beam is merged with a B^{2+} beam selected from an electron cyclotron resonance (ECR) ion source using a 90° analyzing magnet. After traveling in a 68.5-mm-long electric-field-free interaction region and experiencing inelastic as well as elastic collisions, the merged beams enter a second trochoidal analyzer (''demerger'') through a set of five apertures that stop electrons that are elastically scattered at large angles and would otherwise reach the detector. The primary electrons are deflected in the analyzer into a Faraday cup, while the inelastically scattered electrons strike a position-sensitive detector (PSD) consisting of a pair of microchannel plates and a resistive anode. The ion beam, which is not significantly affected by the two trochoidal analyzers, continues to travel through a set of deflectors and is bent by 90° to be collected in the ion Faraday cup. A two-dimensional video probe [10] is used to measure the flux distributions of the electron and the ion beams, and therefore their overlap, at seven positions along the interaction region.

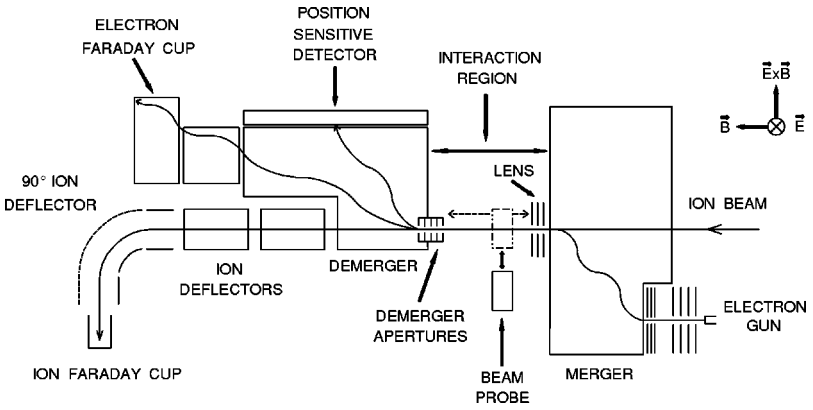

FIG. 1. Schematic diagram of the JILA/ORNL merged electron-ion beam energy loss apparatus. See the text for a description.

Large background count rates at the PSD from interactions of both beams with surfaces and residual gas require a four-way chopping scheme to determine the inelastic signal. The PSD signal is sequentially read through a position computer and a first-in–first-out buffer into four histogram memory modules ($M_1, \ldots, M_4$) by switching the ion and/or electron beam on and off: $M_1 = S + B_e + B_i + B_d$ (both beams on), $M_2 = B_e + B_d$ (electron beam on, ion beam off), $M_3 = B_i + B_d$ (electron beam off, ion beam on), and $M_4 = B_d$ (both beams off), where S, B_i, B_e, and B_d denote the inelastic signal, the ion beam background, the electron beam background, and the dark count rates, respectively. The signal associated with the inelastically scattered electrons is then determined from $S = M_1 - M_2 - M_3 + M_4$. Corrections are made to $M_1, \ldots, M_4$ individually for the dead times of the PSD and the position computer.

The excitation cross section at an interaction energy in the center-of-mass system E_{cm} is given by

$$\sigma(E_{cm}) = \frac{S}{I_e I_i} \frac{qe^2}{\epsilon} \left| \frac{v_e v_i}{v_e - v_i} \right| F, \tag{1}$$

where S is the signal count rate of the inelastically scattered electrons, F is the form factor, ϵ is the PSD detection efficiency, and v_e, v_i, I_e, and I_i are the laboratory velocities and currents of the electrons and the ions of charges e and qe, respectively. The efficiency of the PSD was measured to be 0.481 ± 0.018 in a separate experiment by alternately directing an electron beam of a few femtoamperes onto the PSD and into a Faraday cup connected to a vibrating reed electrometer. From the ratio of the PSD counts and the current in the Faraday cup the efficiency is determined. The form factor F is determined from the electron and the ion beam intensities $G(x,y,z)$ and $H(x,y,z)$:

$$F = \frac{\int G(x,y,z)dx\,dy \int H(x,y,z)dx\,dy}{\int G(x,y,z)H(x,y,z)dx\,dy\,dz}, \tag{2}$$

where z is the direction of the magnetic field.

Before taking data, the electron and the ion beams were tuned to minimize the background counts on the PSD (typically less than 100 counts per nA for each beam). Then the 20-keV ion beam was merged with the electron beam in the interaction region and the form factor F [Eq. (2)] was determined with the video probe. At a particular electron energy, the excitation cross section was measured until a reasonable statistical precision was achieved. Then the apparatus was prepared for the next electron energy by scaling the magnetic field and the voltages of the electron gun, the merger, and the demerger, typically different only by a few percent in order to ensure linearity of scaling and thus to obtain an electron beam with a constant overlap with the ion beam. Before and after determining cross sections at several energies, the form factor was measured and an interpolated value was used to calculate the final cross sections. This procedure ensured that beam fluctuations and the scaling between energies did not change the overlap of the beams significantly during the cross section measurements. The energy region of interest was scanned several times using this method and the results averaged for each energy. The data were fitted to a step function convoluted with a Gaussian distribution at the spectroscopic threshold for the $2s \rightarrow 2p$ transition of 5.998 eV [11]. The data were then corrected by shifting the interaction energy to account for the contact potential and by subtracting the below-threshold contribution to the cross section, assuming this contribution to be independent of energy. The ionization experiment described in Sec. II B showed that a negligible fraction of metastable ions was present in the B^{2+} beam so that no correction to the ion current was needed.

At energies above the transition threshold, inelastically scattered electrons may end up traveling backward in the laboratory frame if the center-of-mass electron velocity in the backward direction is larger than the ion velocity in the forward direction. In this case the electrons do not reach the detector and corrections have to be made [12,13]. Electrons that are velocity matched to 20-keV $^{11}B^{2+}$ ions have an energy of 1.0 eV, so that backscattering corrections were expected to be substantial at energies higher than 1.0 eV above threshold. The corrections were made using SIMION 3D [14], a three-dimensional trajectory modeling program that simulated the demerger region. The resulting detection rates were weighted with the theoretical differential cross sections for this transition. Measurements were not continued to higher energies where corrections were substantial.

In order to raise the interaction energy at which losses remain small, the experiment was repeated with a higher B^{2+} beam energy (36 keV). By this time, however, the condition of the video probe had degenerated to the point that the absolute magnitude of the form factors was unreliable. Hence these results were normalized in absolute magnitude to the results obtained earlier at 20 keV. A normalization factor of 0.895 was obtained as the ratio of the step height of the 20-keV data divided by the step height of the 36-keV data.

B. Ionization

The absolute cross sections for the electron-impact single ionization of $^{11}B^{2+}$ were measured using the ORNL crossed-beams apparatus. This method has been described in detail elsewhere [15–17], so only a brief overview will be given here. The B^{2+} beam was obtained from the same ECR source as for the excitation measurements. Following the analyzing magnet and just before the collision region, the beam was charge purified in an electrostatic parallel-plate analyzer to reject charge-changed ions originating in the beam line. After undergoing ionization in the collision region, the B^{3+} reaction products were separated from the primary B^{2+} beam using a 90° analyzing magnet. The primary beam was directed into a Faraday cup while the product ions were collected in a channeltron electron multiplier after being bent by a 90° electrostatic deflector. As in the excitation experiment described above, a form factor is necessary to quantify the overlap of the two beams. A moveable slit probe was used to measure the vertical intensity distributions necessary to calculate the form factor. The absolute cross sections are then determined from the measurements using

$$\sigma(E_{cm}) = \frac{R}{I_i I_e} \frac{qe^2}{\epsilon} \frac{v_i v_e}{\sqrt{v_i^2 + v_e^2}} F, \tag{3}$$

where R is the product ion count rate, I_i and I_e are the incident ion and electron currents, qe is the charge of the incident ions, v_i and v_e are the incident ion and electron velocities, F is the form factor, and ϵ is the channeltron detection efficiency for the product ions, estimated to be 98% [16]. In this experiment background counts were observed when the ion beam was present but none when only the electron beam was present. Consequently, the electron beam was chopped and the counts from the channeltron were passed to two scalers gated to receive the signal plus background and background, respectively. The signal rate R was derived from the difference between the scaler count rates.

III. IONIZATION THEORY

For a comparison to the present low-energy experimental results, we calculate electron-impact ionization cross sections for B^{2+} using time-independent and time-dependent close-coupling approaches. The time-independent method is based on R-matrix calculations employing a large pseudostate basis in which we aim for convergence in our cross sections to a few percent, while preserving the ability of the R-matrix method to efficiently generate results at many energies. The time-dependent close-coupling method is based on the propagation of wave packets and their projection onto a complete set of bound excited states. The excited-state spectrum is calculated using a pseudopotential for the core electrons. This approach eliminates problems of superelastic scattering and keeps the lattice size relatively small.

A. Time-independent theory

We use an L^2 basis to represent the bound and continuum states of the ion [18]. Excitation of the positive-energy states corresponds to ionization. A more accurate approach, especially at low energies, is to project the positive- *and* negative-energy L^2 states onto the true physical continuum. We use the program AUTOSTRUCTURE [19] to generate an orthogonal set of Laguerre basis orbitals [20]. We use physical orbitals for those states that we wish to study transitions between or from. The N-electron configurations are built up from the one-electron orbitals and then the Hamiltonian is diagonalized to obtain the set of N-electron eigenenergies and eigenstates. For B^{2+}, we use physical $1s$, $2s$, and $2p$ orbitals and pseudoorbitals ($\overline{nl}$) up to $15s$, $14p$, $13d$, $12f$, and $12g$ giving rise to a 55-term close-coupling expansion. Of these, nine of the s, eight of the p, seven of the d, and six each of the f and g pseudoorbitals lie above the ionization limit. A further refinement can be considered. If the initial positioning of the pseudostate term energies is such that one (or more) lies close to the ionization limit then the $\lambda_{\overline{nl}}$ scaling parameters on the Laguerre orbitals [see Eq. (1) of Ref. [20]] can be adjusted (and hence the term energies) to ensure that the ionization limit lies roughly midway between two term energies of the same symmetry, for each symmetry. This reduces the size of the effect of projection, which is an additional approximation. An optimum distribution for B^{2+} was obtained on using the following values for the scaling parameters for the Laguerre orbitals: $\lambda_{\overline{ns}} = 1.15$, $\lambda_{\overline{np}} = 1.04$, $\lambda_{\overline{nd}} = 0.98$, $\lambda_{\overline{nf}} = 0.95$, and $\lambda_{\overline{ng}} = 1.04$. Thus our ($R$-matrix) pseudostate basis is much larger than that of Marchalant *et al.* [7]. They were looking at excitation (up to $n=4$) as well as ionization and so used physical (Hartree-Fock) orbitals up to $n=4$ and pseudo-orbitals up to $9s$, $8p$, $8d$, and $7f$. This limited pseudostate expansion necessitated taking the average of results obtained from five separate R-matrix runs using different scaling parameters. Even so, as Marchalant *et al.* [7] noted, their RMPS results fell significantly below their convergent close-coupling results for ionization at higher energies. In fact, our (R-matrix) calculations are much closer in spirit to their convergent close-coupling calculations.

We solve the time-independent close-coupling equations using the R-matrix method [21]. Our starting point is RMATRX I, the (Breit-Pauli) R-matrix codes [22] developed for the Iron Project [23]. A practical problem encountered is the orthogonalization of the continuum basis orbitals (that are used to describe the scattering electron) to the Laguerre orbitals. Bartschat *et al.* [24] use a numerical Schmidt orthogonalization procedure. We use an alternative approach that we find to be more stable numerically when using a large R-matrix continuum basis [20,25]. For B^{2+}, our ''target'' orbitals necessitate the use of an R-matrix box of radius $R=26.7$ and 30 continuum basis orbitals per angular momentum (initially) to obtain cross sections converged to 1% up to an incident electron energy of 200 eV. We carried out LS-coupling calculations with exchange, as described above, for $L=0-8$ together with a ''top up'' for higher L. The top up merits further discussion. We make use of Seaton's STGF asymptotic code [26]. The original version only topped up dipole transitions in LS coupling, which often suffices for the excitation of physical discrete states. (Later versions in use also top up fine-structure transitions.) This is insufficient for the excitation of pseudostates because there is a bias towards high multipole transitions (in contrast to the normal ''physical'' case). This is due to the fact that unitarity forces con-

vergence of the total cross section (i.e., summed over all $\bar{l}$) before convergence is achieved in the partial cross sections (i.e., each individual $\bar{l}$); see [27] for a detailed study. We find that topping up only the dipole and the quadrupole transitions, for example, gives rise to a severe underestimate of the partial high-L contribution. We have implemented a top up using the lowest positive 2^{λ}-pole for each transition [28] to overcome this.

In our work on Be^{+} [29] we determined the ionization cross section simply by summing-up the cross sections to the positive-energy pseudostates. A more refined treatment was developed for Na-like ions [28] and is applied here to the case of B^{2+}. Following Gallaher [30], we determine our ionization cross section from

$$\sigma_{ion}=\sum_{\bar{n}}\left[1-\sum_{n}|\langle n|\bar{n}\rangle|^2\right]\sigma_{\bar{n}}, \tag{4}$$

where $|\bar{n}\rangle$ denotes a positive- or negative-energy pseudoeigenstate, $\sigma_{\bar{n}}$ is the excitation cross section (from the initial ground state) to $|\bar{n}\rangle$, and $\langle n|$ denotes a physical discrete eigenstate. The $|\bar{n}\rangle$ and $\langle n|$ are themselves configuration-mixed states of the original target basis resulting from diagonalization of the N-electron Hamiltonian. The sum over $\bar{n}$ is dominated by those pseudostates that lie just above and below the ionization limit. The sum over n is over all physical discrete states and its evaluation requires the overlaps between the pseudoorbitals and a Rydberg series of physical orbitals. The point about this (approximate) form of the projection is that it takes place on the cross sections, not the scattering matrix, and so can be applied as a simple postprocessing exercise after STGF has been run. Away from threshold the effect of projection is small for B^{2+}, resulting in a reduction of less than 3%.

B. Time-dependent theory

Direct ionization cross sections for the outer $2s$ subshell of B^{2+} are calculated by direct solution of the time-dependent Schrödinger equation [31,32]. The total wave function is expanded as a product of a two-dimensional radial function and a four-dimensional coupled spherical harmonic. By the variational principle the two-dimensional radial function is found to satisfy a coupled set of time-dependent partial differential equations for each total LS symmetry. Each initial LS radial function is constructed as either a symmetrized product of an incoming radial wave packet for the scattering electron and a bound orbital for the valence electron in the case of singlet spin symmetry or as an antisymmetrized product in the case of triplet spin symmetry. The $1s^2$ core for B^{2+} is represented by an ℓ-dependent pseudopotential [29]. The time-dependent close-coupled equations are then solved by lattice methods employing low-order finite differences. Each two-dimensional radial function is partitioned over the many processors found in a distributed-memory supercomputer. Time propagation of each lattice domain is performed independently with only message passing at the domain boundaries. After the collision the two-dimensional radial functions are projected onto the one-dimensional radial eigenstates for a bound valence electron of B^{2+}. The resulting collision probabilities for elastic scattering and bound-state excitation are then subtracted from one to yield a total ionization cross section.

The $2s$ direct ionization cross section for B^{2+} is calculated at electron-impact energies of 100 eV, 130 eV, and 160 eV. All calculations employed a lattice of 200×200 points with a mesh spacing of $\Delta r=0.2$ a.u. At time zero the incoming radial wave packet representing the scattered electron is a Gaussian of width 5.0 a.u. centered at 20 a.u. from the nucleus. The total time propagation is given by 40 a.u. divided by the group velocity of the wave packet. For an incident energy of 100 eV the total time is 15 a.u., corresponding to 6000 time steps at $\Delta t=0.0025$ a.u. The number of close-coupled equations increases as a function of L. For example, converged results for $L=0$ may be obtained using four close-coupled equations, while converged results for $L=6$ needed 16 coupled channels. Fortunately, the total L partial cross section (singlet plus triplet spin symmetries) calculated using the time-dependent lattice method agree quite well with the corresponding time-independent distorted-wave cross sections at the higher L. Thus we used a hybrid approach in which we added close-coupling results for $L=0-6$ with distorted-wave results for $L=7-30$. The total direct ionization cross sections for B^{2+} at the three incident energies are shown as the cross-haired diamonds in Fig. 3.

IV. RESULTS

A. Excitation

The excitation results are shown in Fig. 2 and are also available in tabulated form [9], with the relative measurements (ion energy 36 keV) normalized to the absolute measurements (ion energy 20 keV). The error bars for the absolute measurements represent the relative uncertainty at the 90% confidence level (C.L.), which is the quadrature sum of the relative uncertainties at the 68% C.L. from the counting statistics and from the relative uncertainties of the form factor (2%), multiplied by 1.7. The error bars for the relative measurements are obtained in a similar manner, but in this case the relative form factor uncertainty is 11%. The outer error bar on the absolute measurement for 6.32 eV represents the total expanded uncertainty at the 90% C.L., which is the quadrature sum of the relative uncertainty and the systematic uncertainty, consisting of the uncertainties of the absolute value of the form factor (8%), spatial delimitation of the signal on the PSD (6%), efficiency (4%), ion and electron beam currents (1% each), and ion beam purity (1%).

Points of both the absolute and relative data sets appear to be at a maximum near 6.2 eV and at a minimum near 6.4 eV. With the uncertainties as large as they are, it is impossible to attach any reality to this suggested structure, but since this trend persisted in many data runs it seems worthwhile calling attention to it. There appears to be no theoretical basis for any resonances in this region.

Also shown in Fig. 2 is an RMPS calculation of Bartschat and co-workers [7,33], convoluted with the experimental energy spread of 0.24 eV and shifted to the spectroscopic threshold. This prediction is in excellent agreement with the present experimental results.

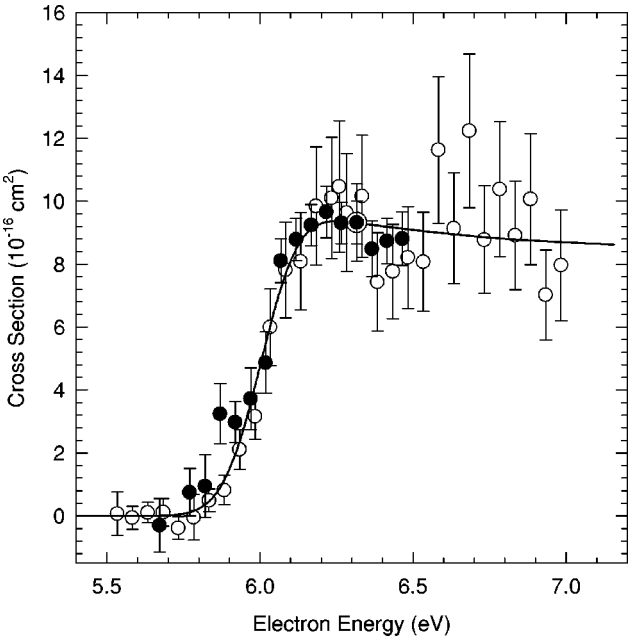

FIG. 2. Cross sections for electron-impact excitation of the $2s \rightarrow 2p$ transition in B^{2+} as a function of the center-of-mass energy. The absolute measurements (20 keV ion energy) are shown as solid circles and the relative measurements (36 keV ion energy) are shown as open circles. The error bars represent the relative uncertainties at the 90% C.L. and the outer error bar on the measurement at 6.32 eV respresents the total expanded uncertainty at the 90% C.L. The RMPS calculation [7,33] is convoluted with an experimentally determined energy resolution of 0.24 eV and represented by the solid line.

B. Ionization

Measured ionization cross sections for electron-impact ionization of B^{2+} are shown, in comparison with other experimental and theoretical results, in Fig. 3 and are also available in tabulated form [17]. In order to be consistent with previous publications in this series of experiments on electron-impact ionization, e.g., [16], the error bars in Fig. 3 represent the relative uncertainty at the 68% C.L., while the tabulated results [17] contain both the relative uncertainty at the 68% C.L. and the total expanded uncertainty at the 90% C.L. The relative uncertainty at the 68% C.L. includes statistical counting uncertainties and a 2% uncertainty from form factor variations, added in quadrature. Systematic uncertainties at the 90% C.L. are as follows: product ion detection and pulse transmission (5%), transmission of product ions to the detector (4%), absolute value of the form factor (4%), electron and ion current measurements (2% each), and electron and ion velocities (1% each). To obtain the total expanded uncertainties for the measurements, the relative uncertainties, multiplied by 1.7 (i.e., at the 90% C.L.) are added in quadrature to the systematic uncertainties. A typical total expanded uncertainty near the peak is 10%.

In Fig. 3 the present experimental and theoretical data [time-dependent close-coupling (TDCC) theory and RMPS theory] are presented and compared with previous data. Very good agreement is found between the experiment and the TDCC theory, while the RMPS theory underestimates the current experiment but still is within the total expanded uncertainty of 10%. The current experiment is consistent with

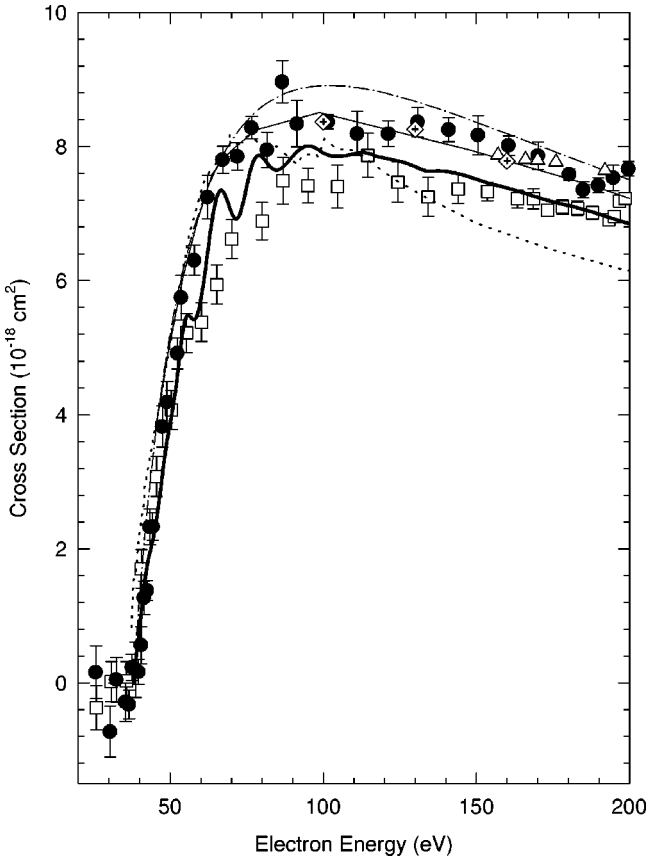

FIG. 3. Cross sections for electron-impact single ionization of B^{2+}. The present experimental results are shown as solid circles with the relative uncertainty at the 68% C.L. The present theory is shown as the cross-haired diamonds (time-dependent close-coupling calculation) and as the thick solid line (R-matrix-with-pseudostates calculation). The dot-dashed line is the distorted-wave-with-exchange theory of Ref. [8]. The thin solid line and the dashed line represent the convergent close-coupling and the RMPS calculations, respectively, of Ref. [7]. The triangles represent the measurements of Ref. [4] and the squares represent the measurements of Ref. [3].

the measurements of Hofmann *et al.* [4] and, to a lesser degree but still within the total expanded uncertainties, also with the measurements of Crandall *et al.* [3]. The distorted-wave-with-exchange (DWE) theory of Younger [8] is about 5% higher than the current experimental data around the peak. Very good agreement over the entire energy range is found between the present experiment and the convergent-close-coupling (CCC) theory of Marchalant *et al.* [7], while agreement with the RMPS calculation of Marchalant *et al.* [7] is limited to the region around the peak.

The characteristic small oscillations in the RMPS results arise from the use of a finite basis to describe the continuum and arise to a greater or lesser extent in all RMPS and CCC calculations. As the basis is extended toward completeness, the oscillations disappear. While other authors smooth them out with various methods, we prefer to show the raw results. It is clear to the eye where a least-squares fitted curve would lie.

V. CONCLUSIONS

For B^{2+}, absolute electron-impact excitation cross sections for the $2s\,^2S \rightarrow 2p\,^2P$ transition and absolute electron-

impact ionization cross sections have been measured. The RMPS calculation of Bartschat and co-workers [7,33] is in very good agreement with the present excitation cross sections.

Excellent agreement has been found between the present ionization measurements and the present TDCC calculation and also with the CCC calculation of Marchalant *et al.* [7]. The data are also in good agreement with the measurements of Hofmann *et al.* [4], which are at the higher energies of the present measurements. Both the TDCC and RMPS calculations show a reduction in the ionization cross section as calculated by distorted-wave theory. The difference in the two close-coupling calculations is just within the overall numerical uncertainties found in these quite different approaches. Although agreement is not as good with the present RMPS calculation as with the TDCC calculations, the current measured data are still consistent with this calculation within the total expanded uncertainty as it is also with the DWE calculation of Younger [8]. The present measurements at the peak of the cross section are about 14% higher than the earlier measurements of Crandall *et al.* [3], but again this is within the combined total expanded uncertainties of the measurements.

ACKNOWLEDGMENTS

The authors wish to thank J. W. Hale for skilled technical assistance. This work was supported in part by the Office of Fusion Energy Sciences of the U.S. Department of Energy under Contract No. DE-A102-95GR54293 with the National Institute of Standards and Technology and Contract No. DE-AC05-96OR22464 with Lockheed Martin Energy Research Corp. M.S.P. was supported by a U.S. Department of Energy grant (No. DE-FG05-96-ER54348) with Auburn University. The time-dependent calculations were carried out on the Cray T3E-600 computer at the National Energy Research Supercomputer Center in Berkeley, California.

[1] D. H. Crandall, R. A. Phaneuf, and P. O. Taylor, Phys. Rev. A **18**, 1911 (1978).
[2] D. C. Gregory, G. H. Dunn, R. A. Phaneuf, and D. H. Crandall, Phys. Rev. A **20**, 410 (1979).
[3] D. H. Crandall, R. A. Phaneuf, D. C. Gregory, A. M. Howald, D. W. Mueller, T. J. Morgan, G. H. Dunn, D. C. Griffin, and R. J. W. Henry, Phys. Rev. A **34**, 1757 (1986).
[4] G. Hofmann, A. Müller, K. Tinschert, and E. Salzborn, Z. Phys. D **16**, 113 (1990).
[5] E. W. Bell, X. Q. Guo, J. L. Forand, K. Rinn, D. R. Swenson, J. S. Thompson, G. H. Dunn, M. E. Bannister, D. C. Gregory, R. A. Phaneuf, A. C. H. Smith, A. Müller, C. A. Timmer, E. K. Wåhlin, B. D. DePaola, and D. S. Belić, Phys. Rev. A **49**, 4585 (1994).
[6] M. E. Bannister, Y.-S. Chung, N. Djurić, B. Wallbank, O. Woitke, S. Zhou, G. H. Dunn, and A. C. H. Smith, Phys. Rev. A **57**, 278 (1998).
[7] P. J. Marchalant, K. Bartschat, and I. Bray, J. Phys. B **30**, L435 (1997).
[8] S. M. Younger, J. Quant. Spectrosc. Radiat. Transf. **26**, 329 (1981).
[9] http://www-cfadc.phy.ornl.gov/meibel/.
[10] J. L. Forand, C. A. Timmer, E. K. Wåhlin, B. D. DePaola, G. H. Dunn, D. Swenson, and K. Rinn, Rev. Sci. Instrum. **61**, 3372 (1990).
[11] C. E. Moore, *Atomic Energy Levels*, Natl. Bur. Stand. (U.S.) Circ. No. 35 (U.S. GPO, Washington, DC, 1971), Vol. 1.
[12] Y.-S. Chung, N. Djurić, B. Wallbank, G. H. Dunn, M. E. Bannister, and A. C. H. Smith, Phys. Rev. A **55**, 2044 (1997).
[13] X. Q. Guo, E. W. Bell, J. S. Thompson, G. H. Dunn, M. E. Bannister, R. A. Phaneuf, and A. C. H. Smith, Phys. Rev. A **47**, R9 (1993).
[14] SIMION 3D, Version 6.0, David A. Dahl, Idaho National Engineering Laboratory.
[15] M. E. Bannister, F. W. Meyer, Y.-S. Chung, N. Djurić, G. H. Dunn, M. S. Pindzola, and D. C. Griffin, Phys. Rev. A **52**, 413 (1995).
[16] M. E. Bannister, Phys. Rev. A **54**, 1435 (1996).
[17] http://www-cfadc.phy.ornl.gov/xbeam/.
[18] H. A. Yamani and W. P. Reinhardt, Phys. Rev. A **11**, 1144 (1975).
[19] N. R. Badnell, J. Phys. B **19**, 3827 (1986).
[20] N. R. Badnell and T. W. Gorczyca, J. Phys. B **30**, 2011 (1997).
[21] P. G. Burke and K. A. Berrington, *Atomic and Molecular Processes — An R-Matrix Approach* (IOP, Bristol, 1993).
[22] K. A. Berrington, W. B. Eissner, and P. H. Norrington, Comput. Phys. Commun. **92**, 290 (1995).
[23] D. G. Hummer, K. A. Berrington, W. Eissner, A. K. Pradhan, H. E. Saraph, and J. A. Tully, Astron. Astrophys. , **279**, 298 (1993).
[24] K. Bartschat, E. T. Hudson, M. P. Scott, P. G. Burke, and V. M. Burke, J. Phys. B **29**, 115 (1996).
[25] T. W. Gorczyca and N. R. Badnell, J. Phys. B **30**, 3897 (1997).
[26] K. A. Berrington, P. G. Burke, K. Butler, M. J. Seaton, P. J. Storey, K. T. Taylor, and Yu Yan, J. Phys. B **20**, 6379 (1987).
[27] I. Bray, Phys. Rev. Lett. **73**, 1088 (1994).
[28] N. R. Badnell, M. S. Pindzola, I. Bray, and D. C. Griffin, J. Phys. B **31**, 911 (1998).
[29] M. S. Pindzola, F. Robicheaux, N. R. Badnell, and T. W. Gorczyca, Phys. Rev. A **56**, 1994 (1997).
[30] D. F. Gallaher, J. Phys. B **7**, 362 (1974).
[31] M. S. Pindzola and D. R. Schultz, Phys. Rev. A **53**, 1525 (1996).
[32] M. S. Pindzola and F. Robicheaux, Phys. Rev. A **54**, 2142 (1996).
[33] K. Bartschat (private communication).